Scientific Research Publishing

Journal of Water Resource and Protection, 2023, 15, 539-556
https://www.scirp.org/journal/jwarp
ISSN Online: 1945-3108
ISSN Print: 1945-3094

Estimation of the Actual Evapotranspiration by the SEBAL Method in the Irrigated Rice Perimeter of Zatta (Yamoussoukro—Côte d'Ivoire)

Junias Léandre Kra[1], Moïse Botou Adahi[2], Brice Arthur Konan-Waidhet[1], Jean-Yves Konan N'Guessan[1], Joël Doyéré Koné[2], Emmanuel Nogbou Assidjo[3]

[1]Department of Geosciences and Environment, Université Jean Lorougnon Guédé (UJLoG), Daloa, Côte d'Ivoire
[2]Department of Rural Engineering and Geographical Sciences, Institut National Polytechnique Félix Houphouët-Boigny (INP-HB), Yamoussoukro, Côte d'Ivoire
[3]Department of Chemical and Food Engineering, Institut National Polytechnique Félix Houphouët-Boigny (INP-HB), Yamoussoukro, Côte d'Ivoire
Email: junias.kra@ujlg.edu.ci

How to cite this paper: Kra, J.L., Adahi, M.B., Konan-Waidhet, B.A., N'Guessan, J.-Y.K., Koné, J.D. and Assidjo, E.N. (2023) Estimation of the Actual Evapotranspiration by the SEBAL Method in the Irrigated Rice Perimeter of Zatta (Yamoussoukro—Côte d'Ivoire). *Journal of Water Resource and Protection*, **15**, 539-556.
https://doi.org/10.4236/jwarp.2023.1510030

Received: May 13, 2023
Accepted: October 23, 2023
Published: October 26, 2023

Abstract

In this study, the SEBAL (Surface Energy Balance Algorithm for Land) model was used to map the spatio-temporal distribution of actual evapotranspiration in the Yamoussoukro department (Côte d'Ivoire). Like other regions of the country, the Yamoussoukro district is confronted with the phenomenon of evapotranspiration (ET). This is a very important component that comes into play in the water balance but also in the calculation of the water needs of agricultural crops. Consequently, its estimation is of paramount importance in research related to the rational management of water resources, particularly agricultural water. The objective of this study was to analyze the spatio-temporal distribution of actual evapotranspiration (AET) as a function of land cover and land use. The methodology used is based on the SEBAL model which uses remote sensing (Landsat 8_OLI/TIRS) and climatic data to estimate actual evapotranspiration and analyze the spatio-temporal distribution of AET. The results reveal that the AET varied from 0 to 5.44 mm/day over the period from December 2019 to February 2020 with an average value of 4.92 mm/day. The highest average values occurred for water bodies (4.90 mm/day) and flooded vegetation (4.88 mm/day) while the lowest values occurred in residential areas (2.04 mm/day). Furthermore, the results show that the difference between the SEBAL model and the FAO-Penman-Monteith method is minimal with an average RMSE of 0.36 mm/day for all the satellite images. This study demonstrates the considerable potential of remote sensing for the characterization and estimation of spatial evapotranspiration in the

Zatta irrigated rice-growing area.

Keywords

Evapotranspiration, Water Balance, Rational Management, Remote Sensing, SEBAL Model

1. Introduction

One of the main problems faced by most actors in the rice sector is the efficient use of available water resources for crop irrigation. In this sense, a rational management of these water resources for rice production remains the only solution to overcome this problem.

Like many countries, Côte d'Ivoire is experiencing strong population growth based on a high average annual growth rate of 2.9%, high immigration of 22% and a high rate of urbanization of 48.8% [1]. Rice, with its culinary assets, is the most consumed cereal in this country [2] and is one of the staple foods of the majority of the population [3]. However, rice is one of the most water-intensive crops. Therefore, reducing irrigation water consumption while increasing rice yields has become an urgent problem to be solved. Yamoussoukro, with its eight peri-urban areas, including that of Zatta, also with dams, offers an appropriate framework for the analysis of this problem.

Indeed, evapotranspiration (ET) is one of the key factors in water balance and water resources management [4] [5]. It is also important that this component be estimated with precision, as it is an indicator of the water resources available in an area [6]. In addition, food demand and wealth creation from agriculture are important reasons for understanding and control evapotranspiration. Thus, water management through the understanding of evapotranspiration is of great interest in developing countries, including Côte d'Ivoire.

In recent years, several studies have been carried out to shed light on the phenomenon of evapotranspiration [7] [8] [9]. Most of these studies have used expensive if not limited, methods [10] as they only provide point values.

In contrast, the SEBAL (*Surface Energy Balance Algorithm for Land*) method coupled with remote sensing data is more promising since the model estimates ET at large spatial scales and uses a small amount of climate data [11]. The SEBAL method is robust and has been widely used and validated worldwide [12] [13] [14] [15]. However, no study using SEBAL method has yet been carried out in the department of Yamoussoukro (Côte d'Ivoire) which serves as the study site.

Considering the water-related issues and the problems mentioned above, knowledge of evapotranspiration values for different types of land use is necessary to help in water resources management. Therefore, the general objective of this study is to analyze the spatial distribution of actual evapotranspiration in the area of the irrigated rice perimeter of Zatta (Yamoussoukro, Côte d'Ivoire) using the SEBAL model (Surface Energy Balance Algorithm for Land).

2. Materials and Methods

2.1. Study Area

This study was conducted in the irrigated rice perimeter of Zatta. Zatta is a village in the center of Côte d'Ivoire in the department and autonomous district of Yamoussoukro. This district is located more at coordinates 06˚49' and 06˚47' North latitude and 05˚16' and 05˚15' West longitude (Figure 1) and covers an area of 3500 km^2. It benefits from a hydrographic network essentially composed of the Marahoue (Red Bandama) and the N'Zi, two tributaries of the Bandama. The climate in this area is of the attenuated transition equatorial type, characterized by more or less moderate solar radiation, a dry season with an average temperature of around 25.8˚C and a rainy season marked by an annual rainfall of the order of 1145.60 mm (Figure 2). I' average annual relative humidity is 78.3% and wind speed 1.5 m/s. The relief is made up of plains and plateaus spread out between 200 and 500 m, separated from each other by a low slope of 10 to 30 m.

2.2. Data Used

2.2.1. Climatic Data

The climatic data used are from the meteorological station of SODEXAM (Company of Exploitation and Development and Airport, Aeronautics and Meteorology). This station is located at 06˚54'11" North Latitude and 05˚21'18" Longitude and at an altitude of 213.05 m. These data are collected on a daily basis and include several variables including air temperature, wind speed and relative humidity.

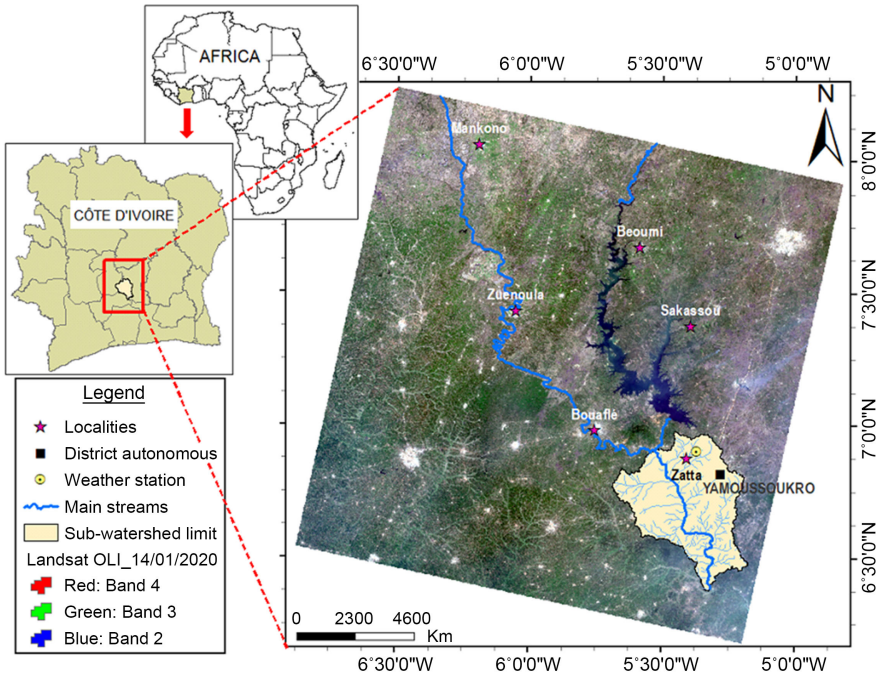

Figure 1. Location of the study area.

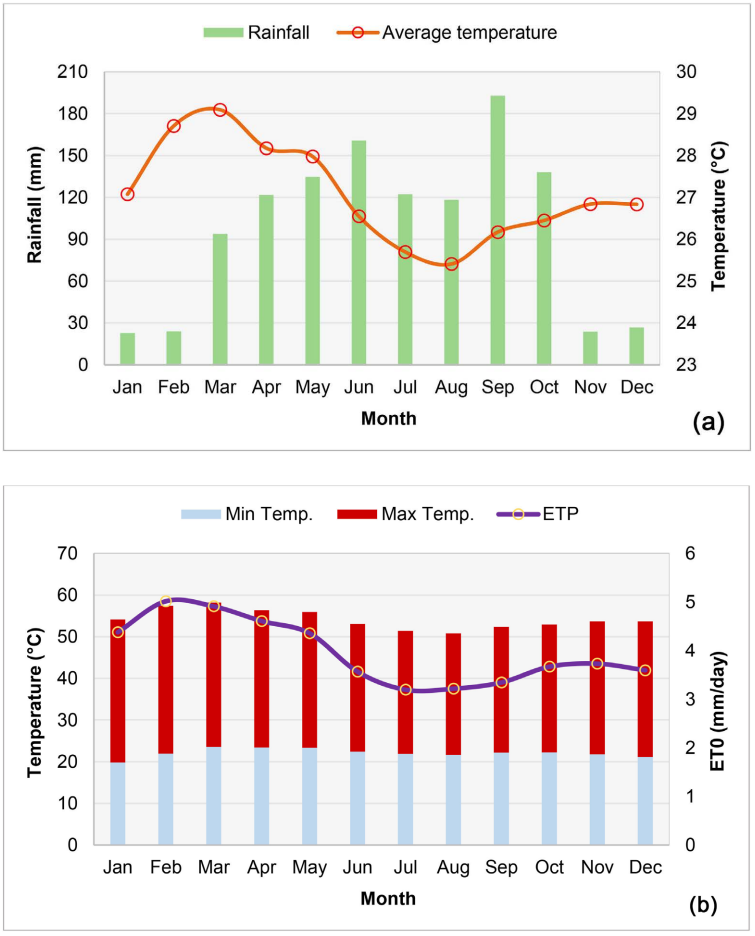

Figure 2. Precipitation, temperature and total evapotranspiration of the study area during the rice growth cycle from 2019 to 2020.

2.2.2. Satellite Data

They are represented by four (4) Landsat 8 OLI/TIRS type images acquired during the rice growth period (2019-2020) on the dates 29 December 2019, 14 January 2020, 30 January 2020 and February 15, 2020 and a digital terrain model (DTM). The four images consist of eleven (11) spectral bands in the visible, infrared and thermal infrared range. They were downloaded free of charge from the United States Geological Survey (USGS) site, considering low cloud cover. The characteristics of the images studied are presented in **Table 1**.

As for the digital terrain model (DTM), it comes from SRTM (Shuttle Radar Topography Mission) and was downloaded from the website: https://earthexplorer.usgs.gov. It is a 30 m resolution image data used to consider topographic effects (slope and elevation) in order to estimate the net radiation reaching the ground surface.

2.2.3. Classification of Land Use and Cover

In order to estimate the actual evapotranspiration for the different types of land use and land cover in the Zatta hydro-agricultural scheme area, we used a global land cover map provided by the study of [16]. It is a composite of ten (10) land

cover classes produced by a deep learning model using ground-sampled image pixels with an overall accuracy of 86% (Figure 3). Seven (7) main covers were chosen for the analysis of the estimated AET: 1) water, 2) vegetation, 3) flooded vegetation, 4) cropland, 5) grassland, 6) shrub and 7) bare and built ground.

Table 1. Main characteristics of Landsat OLI/TIRS satellite images.

Band	Name of the band	Spectral range (μm)	Spatial resolution (m)
1	Aerosol	0.435 - 0.451	
2	Blue	0.452 - 0.512	
3	Green	0.533 - 0.590	
4	Red	0.636 - 0.673	30
5	Near infrared	0.851 - 0.879	
6	SWIR 1	1.566 - 1.651	
7	SWIR 2	2.107 - 2.294	
8	Panchromatic	0.503 - 0.679	15
9	Cirrus	1.363 - 1.384	30
10	TIR 1	10.60 - 11.19	100
11	TIR 2	11.50 - 12.51	

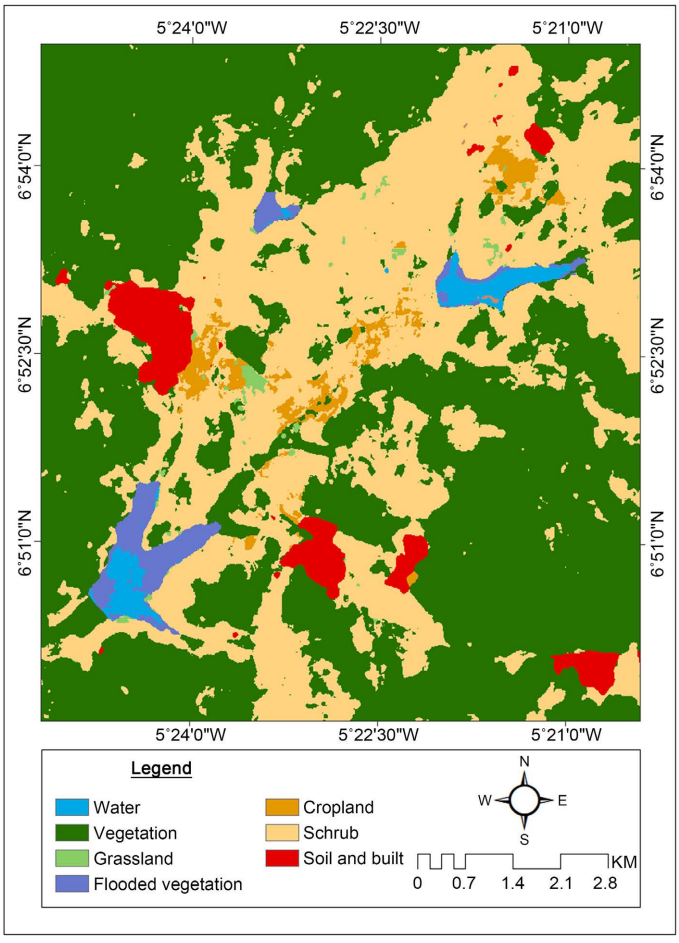

Figure 3. Classification of land use and land cover in the Zatta rice perimeter area [16].

2.3. The SEBAL Model

In this study, the SEBAL model was used to spatially estimate the real evapotranspiration of a canopy. Indeed, SEBAL is an image processing model based on the energy balance equation at the surface of the earth and which calculates the ET as well as other energy values. The principle is that, during a given time interval, the energy which arrives at the surface of a cover is equal to the energy which leaves the same surface. According to [17], the equation for a given surface is written as follows:

$$\lambda ET = R_n - G - H \tag{1}$$

where λET: the latent heat flux (representing the fraction of evapotranspiration in $W \cdot m^{-2}$); R_n: the net radiation ($W \cdot m^{-2}$); G: ground heat flux ($W \cdot m^{-2}$); H: the sensible heat flux ($W \cdot m^{-2}$).

The conceptual diagram of the SEBAL model used in this study is shown in Figure 4.

For the use of the SEBAL model, it is first necessary to correct the atmospheric effect for each of the spectral bands of the satellite images due to a disturbance during the recording of the light signal. Atmospheric corrections consist of the extraction of this signal, information that does not depend on the effects of the atmosphere [18]. Atmospheric corrections are made in order to transform the raw numerical values of the images in ground reflectance values. For this purpose, we used the FLAASH model (Fast Line-of-sight Atmospheric Analysis of Spectral Hypercubes) of the ENVI software which very easily performs these corrections and which integrates a radiation transfer code [19].

2.4. Estimation of Evapotranspiration

As mentioned above, estimating evapotranspiration amounts to solving the surface energy balance equation by determining its different components.

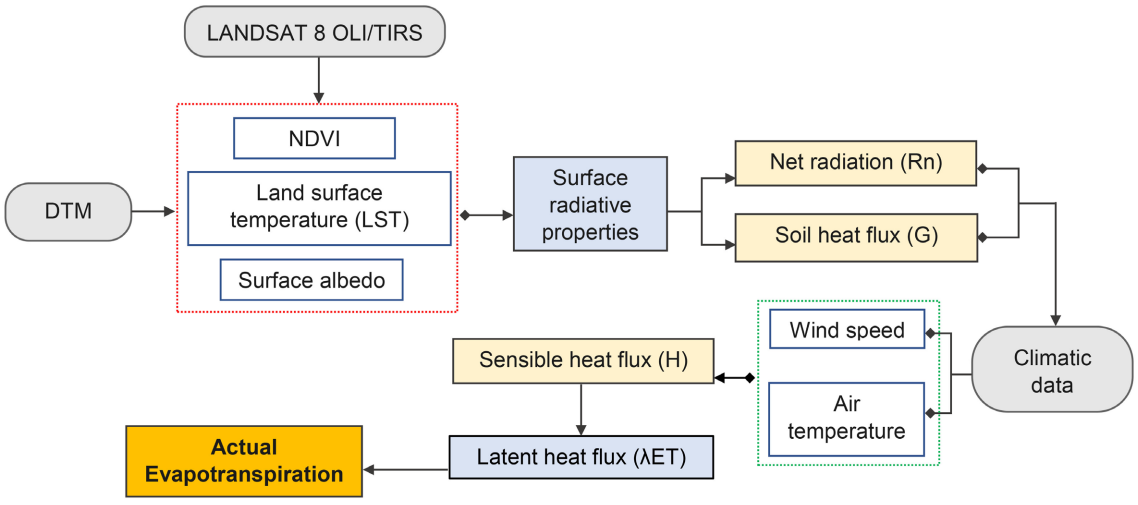

Figure 4. Flowchart of the SEBAL model which uses remote sensing and climate data to estimate actual evapotranspiration.

2.4.1. Net Radiation (R_n)

Net radiation (R_n) represents the radiative energy balance at the earth's surface. This balance involves the albedo (α), the surface emissivity (ε_s), incoming short wavelength radiation ($R_s^{\downarrow}$), outgoing ($R_L^{\uparrow}$) and incoming ($R_L^{\downarrow}$) long wavelength radiation at ground level [20]:

$$R_n = (1-r_0)R_S^{\uparrow} + R_L^{\downarrow} - R_L^{\uparrow} - (1-\varepsilon_s)R_L^{\downarrow} \quad (2)$$

The incoming short wavelength atmospheric radiation is given by the following formula:

$$R_S^{\downarrow} = G_{SC} \times \cos\theta \times d_r \times \tau_{sw} \quad (3)$$

where G_{sc}: the solar constant; $\cos\theta$: the cosine of the angle of solar incidence, d_r: inverse of the square of the relative Earth-Sun distance, τ_{sw}: the transmissivity of the atmosphere.

Incoming long-wavelength atmospheric radiation can be estimated from the air temperature (T_a), the emissivity of the atmosphere (ε_a) and the Stephan-Boltzmann constant (σ) [21]. Atmospheric radiation is expressed according to the following relationship:

$$R_L^{\downarrow} = \varepsilon_a \times \sigma \times T_a^4 \quad (4)$$

The terrestrial radiation emitted from a tracked pixel is estimated by also applying the Stephan-Boltzmann formula:

$$R_L^{\uparrow} = \varepsilon_s \times \sigma \times T_s^4 \quad (5)$$

where T_s is the surface temperature:

$$T_s = \frac{T_b}{1 + \frac{\lambda \times T_b}{C_2} \times \ln \varepsilon_s} \quad (6)$$

where T_b: the brightness temperature of the sensor; C_2: the product of Planck's constant ($h = 6.626 \times 10^{-34}$ J s) and Boltzmann's constant related to the speed of light ($c = 2.998 \times 108$ m/s); λ: is the wavelength of the emitted radiance (μm); h: is Planck's constant (6.626×10^{-34} J/s).

2.4.2. Soil Heat Flux (G)

The heat flux in the soil is estimated from the empirical formula of [22] cited by [20] [21]. This expression considers surface temperature (T_s), albedo (α), normalized difference vegetation index ($NDVI$) and net radiation (R_n):

$$\frac{G}{R_n} = \frac{T_s}{\alpha}\left[0.0038\alpha + 0.007\alpha^2\right]\left[1 - 0.98NDVI^4\right] \quad (7)$$

Albedo (α) is the ratio of reflected radiation to incident radiation. It is calculated by the expression proposed by [23]:

$$\alpha = 0.356 \times r_2 + 0.13 \times r_4 + 0.373 \times r_5 + 0.085 \times r_6 + 0.072 \times r_7 - 0.0018 \quad (8)$$

where r_2, r_4, r_5 are respectively the reflectances in the blue, red, near infrared channels and r_6, r_7 the reflectances in the short infrared of the sensor.

As for the vegetation index (*NDVI*), its calculation involves the reflectances in the red (r_4) and near infrared (r_5) channels according to [24]:

$$NDVI = \frac{r_5 - r_4}{r_5 + r_4} \tag{9}$$

2.4.3. Sensible Heat Flux (*H*)

The sensible heat flux (*H*) corresponds to the transfer of heat by convection between the surface and the air [25] expressed by the equation below:

$$H = \frac{\rho C_p}{r_{ah}} dT \tag{10}$$

where ρ and C_p are respectively the density of air and the specific heat of air at constant pressure (1004 $J \cdot kg^{-1} \cdot K^{-1}$); dT: the temperature difference T_1 and T_2 between two atmospheric levels z_1 and z_2 (generally at 0.1 and 2 m from the ground respectively); r_{ah}: the aerodynamic resistance to heat transfer [26].

Since the temperature difference and the aerodynamic resistance are unknown, an iteration process described by [27] is used to calculate the sensible heat flux (*H*). To facilitate solving the equation, we choose two pixels (hot pixel and cold pixel) in the studied area where reliable values of *H* and *dT* can be predicted. The hot pixel includes dry, uncultivated land. The ET is assumed to be zero in the hot pixel. The cold pixel should be selected in well-irrigated and fully vegetated agricultural fields.

Indeed, the aerodynamic resistance is a function of the wind speed, the thermal stability regime and the surface roughness. Several approaches have been used to estimate the aerodynamic resistance, including [28]. These approaches are mainly based on the use of logarithmic profiles of mass and energy transfer in the surface boundary layer and on the surface-surface boundary layer coupling which takes place at the level of the fluxes at the base of the convective boundary layer [25]. According to [27], the aerodynamic resistance to heat transport (r_{ah}) is calculated as follows:

$$r_{ah} = \frac{\ln\left(\frac{z_2}{z_1}\right) - \psi_{h(z_2)} + \psi_{h(z_1)}}{ku^*} \tag{11}$$

where u^* is friction velocity (m/s) which quantifies turbulent velocity fluctuations in air, k is Von Karman's constant (≈0.41), ψ_m and ψ_h are respectively stability correction functions for the transport of momentum and heat.

$$u^* = \frac{ku_{200}}{\ln\left(\frac{200}{z_{om}}\right) - \psi_m(200\,\mathrm{m})} \tag{12}$$

where u_{200} is the wind speed (m/s) at the mixing height 200 meter, z_{om} is the roughness length and ψ_m (200 m) is the stability correction function for momentum transport at 200 meters from the floor.

The determination of the sensible heat flux also requires the calculation of the

surface temperature difference dT for each pixel. Assuming a linear relationship between dT and T_s [29]:

$$dT = aT_s + b \tag{13}$$

where a and b are correlation coefficients calculated by definition of pixel properties in extreme water conditions.

2.5. Estimation and Spatialization of Evapotranspiration

The AET is determined from the residual term in the energy balance equation. In the first step, the evapotranspiration at the time of the satellite pass (ET_{inst}) is calculated for each pixel contained in the image according to the equation below. It also corresponds to the hourly evapotranspiration:

$$ET_{inst} = 3600\frac{\lambda ET}{\rho_e \lambda} \tag{14}$$

where ρ_e is the density of water (1000 kg/m^3) and λ is the latent heat of vaporization (J/kg).

The daily estimate of the actual evapotranspiration is more practical than the instantaneous actual evapotranspiration. The SEBAL model calculates the real daily evapotranspiration by assuming that the fraction of the reference evapotranspiration (ETF_r = ratio between the instantaneous ET and the reference ET calculated by the climatic data) is an average fixed in 24 hours [20]. The daily ET is given by the equation proposed by [26]:

$$AET_{s,i} = ETF_r \times ET_0 \tag{15}$$

A reference evapotranspiration value (ET_0) can be obtained by the FAO Penman-Monteith formula according to the following relationship:

$$ET_0 = \frac{0.408\Delta\left(R_n - G\right) + \gamma\dfrac{900}{T+273}u_2\left(e_s - e_a\right)}{\Delta + \gamma\left(1 + 0.34u_2\right)} \tag{16}$$

where T: mean daily air temperature at a height of 2 m in (˚C); γ: psychometric constant (kPa·˚C^{-1}); u_2: wind speed at 2 m height; e_s: saturation vapor pressure in kPa; e_a: actual vapor pressure in kPa; $e_s - e_a$: saturation vapor pressure deficit in kPa.

In this study, the spatial estimation of AET is automated using open-source image processing. ENVI 5.1 and GRASS GIS 7.8.7 software were used in the SEBAL model process and the maps were produced by QGIS 3.22.13 software.

2.6. Evaluation of the SEBAL Model

An evaluation of the model is necessary in order to know its performance but also to appreciate and/or judge its capacity to best represent a phenomenon. The evaluation of the results of the SEBAL model was done by comparing the evapotranspiration values simulated by the model and those obtained from the FAO-Penman-Monteith method [15] [30] in the rice-growing area of Zatta on the dates of acquisition of the satellite images.

In this study, four (4) statistical parameters were used to evaluate the performance of the SEBAL model, in particular the root mean quare error (*RMSE*). It measures the difference between the predicted values and the observed values. The lower the value of the *RMSE*, close to zero, the better the model evaluated in terms of accuracy [31]:

$$RMSE = \sqrt{\frac{1}{N}\sum_{i=1}^{N}\left(S_i - O_i\right)^2} \quad (17)$$

where O_i representing the observed values of the FAO-Penman-Monteith equation, S_i representing the estimated values of the SEBAL algorithm; and O_i and S_i are the mean values of the FAO-Penman-Monteith model and SEBAL, respectively.

3. Results and Discussion

Figure 5 illustrates the spatial distribution of evapotranspiration estimated by the SEBAL model on the dates of 29 December 2019, 14 January 2020, 30 January 2020 and 15 February 2020. For all these images, the estimated evapotranspiration values range from 0 to 5.44 mm/day with an average value of 4.92 mm/day. [32] and [33], using MODIS images and the SEBAL model, obtained an average evapotranspiration value equal to 4.9 mm/day on the left bank of Udawalawe in southeastern Sri Lanka and 3.30 mm/day in the Indo-Gangetic Basin, respectively. According to [17], evapotranspiration is determined by meteorological parameters, crop characteristics, management and environmental aspects, and these parameters could explain the average values obtained for the set of satellite images. Furthermore, the analysis of Figure 5 shows that at the rice-growing perimeter, the AET values range between 2.80 and 4.69 mm/day. These values are maximum on 30 January 2019 and minimum on 15 February 2020.

Table 2 presents the values of the statistical parameters calculated from the actual evapotranspiration maps of the area of the irrigated rice perimeter of Zatta. The average of actual evapotranspiration for all the images varies from 2.69 to 3.30 mm/day with a coefficient of variation (CV) between 23.65% and 53.90%. Indeed, the CV evaluates the degree of variability of the data compared to the average. The higher the CV, the greater the dispersion around the mean.

Table 2. Statistical parameters of the spatial variation of the real evapotranspiration in the study area.

Date	Actual evapotranspiration		
	μ (mm)	σ (mm)	CV (%)
29 December 2019	2.96	0.70	23.65
14 January 2020	3.26	1.06	32.52
30 January 2020	3.30	1.08	32.73
15 February 2020	2.69	1.45	53.90

μ = mean; σ = standard deviation; CV = coefficient of variation.

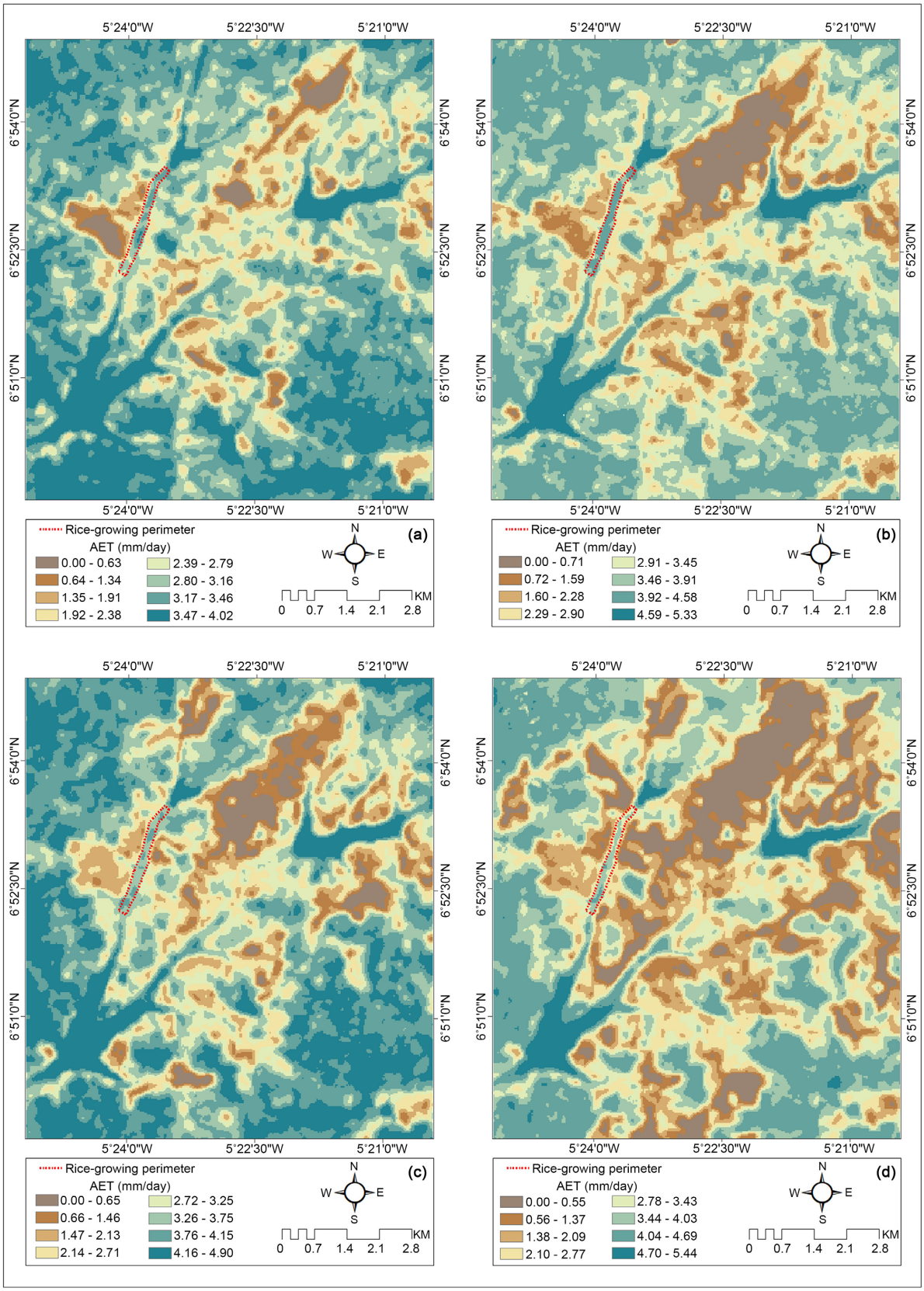

Figure 5. Spatio-temporal variation of actual evapotranspiration by SEBAL on the dates of 29 December 2019 (a), 14 January 2020 (b), 30 January 2020 (c) and 15 February 2020 (d).

Table 3 and Figure 6 shows the distribution of the average actual evapotranspiration values for the land cover types in the study area. These values were obtained by overlaying the land cover and occupation map and the average actual evapotranspiration map of the four (4) satellite images. The graph associates higher values at water bodies (4.90 mm/day) and flooded vegetation values (4.88 mm/day) close to these, while lower values are observed for bare and built-up soils (2.04 mm/day). This result is consistent with many studies, including [12], [34]. da Silva, *et al.* [11] report that the predominant process at the water surface is evaporation and that dense and quality vegetation would be synonymous with higher evapotranspiration than in other types of cover [35] which could justify these values obtained. Moreover, unlike water bodies, evaporation and plant transpiration are the prevailing processes in the vegetation cover. Evapotranspiration is mainly influenced by water availability, but also by solar energy [36].

Table 3. Spatial distribution of actual evapotranspiration according to the type of land cover.

Land cover type	Area (ha)	Area (%)	Average AET (mm/day)
Water	109.13	1.24	4.90
Vegetation	4,874.36	55.28	4.61
Flooded vegetation	35.55	0.40	4.88
Cropland	149.24	1.69	4.51
Grassland	164.36	1.86	2.73
Shrub	3,202.80	36.32	2.88
Soil and built	281.67	3.19	2.04

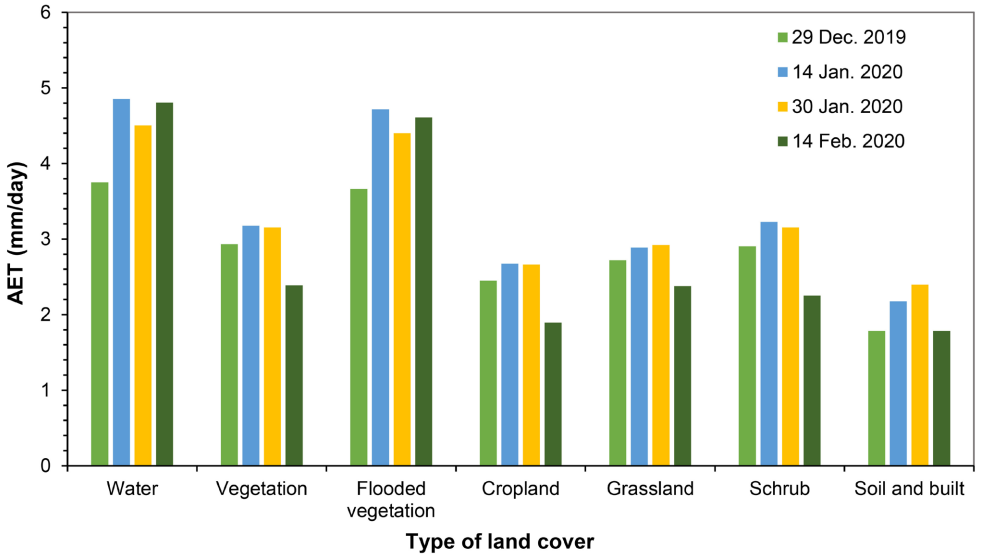

Figure 6. Histogram of the distribution of real evapotranspiration in the area of the irrigated rice perimeter of Zatta.

Concerning cultivated lands and mainly irrigated rice cultivation, they had a actual evapotranspiration lower than those of water bodies and flooded vegetation with an average value of 3.53 mm/day for all satellite images. From the 14th day to the 46th day of the year 2020, the evapotranspiration gradually decreased partly due to the crop development. Indeed, the average development cycle of irrigated lowland rice in the study area is about 120 days and can be divided into three (3) main phases: the vegetative, reproductive and maturation phase [37]. At maturity, the crop's water requirements decrease, the rice fields are less irrigated and therefore less flooded, which could explain the progressive decrease in rice evapotranspiration during this growth period. The values went from 4 mm/day to 3.48 mm/day with a coefficient of variation between 7.5% and 12.36%. The average rice evapotranspiration for all of these images is 3.53 mm/day (**Table 4**).

Figure 7 shows the results of the estimated evapotranspiration from the SEBAL model (ET_SEBAL) for the four (4) satellite images compared to the evapotranspiration of rice according to the FAO method (ET_FAO). The ET_SEBAL values of all pixels on 29 December 2019 were higher than the ET_FAO value (2.91 mm/day) and according to **Table 5**, this image had a lower average relative and absolute error (15.12% and 0.44 mm/day). As for the ET_SEBAL values of all the pixels of 14, 30 January 2020 and 15 February 2020, they are all higher than the evapotranspiration of the rice crop with respective relative and absolute errors of (7.16%; 0.32 mm/day), (8.91%; 0.36 mm/day) and (22.17%; 1 mm/day). Moreover, it is observed that the lower relative errors were 7.16% (14 January 2020) and 8.91% (30 January 2020). These results are consistent with those obtained by [38], on 13 August 2007 (6.88%) and August 06, 2007 (9.01%), for the cultivation of beans in the Entre Ribeiros stream and Preto river sub-basins, between the states of Goiás and Minas Gerais. It appears that the results are quite consistent, since in all days the absolute errors between the evapotranspiration values were less than 0.5 mm/day with the exception of 15 February 2020. de Lima, *et al.* [5] found similar absolute errors when the SEBAL method was compared to the Bowen ratio. For all the images, the RMSE values are between 0.10 and 1 mm/day. Ghaderi, *et al.* [15] reports that an RMSE =

Table 4. Actual evapotranspiration of irrigated rice in the Zatta hydro-agricultural development area.

Date	Actual evapotranspiration of rice				
	Min	Max	μ	σ	CV (%)
29 December 2019	1.96	3.50	3.05	0.27	8.85
14 January 2020	2.76	4.56	4	0.30	7.5
30 January 2020	2.68	4.12	3.60	0.23	6.69
15 February 2020	2.04	4.33	3.48	0.43	12.36

Min = minimum; Max = maximum; μ = mean; σ = standard deviation; CV = coefficient of variation.

Table 5. Statistical values of the comparison between evapotranspiration according to the SEBAL model and the FAO method.

Date	ET_FAO	ET_SEBAL	AE (mm/day)	RE (%)	RMSE (mm/day)
29 December 2019	2.91	3.35	0.44	15.12	0.19
14 January 2020	4.47	4.15	0.32	7.16	0.10
30 January 2020	4.04	3.68	0.36	8.91	0.13
15 February 2020	4.51	3.51	1.00	22.17	1.00

EA = absolute error; ER = relative error.

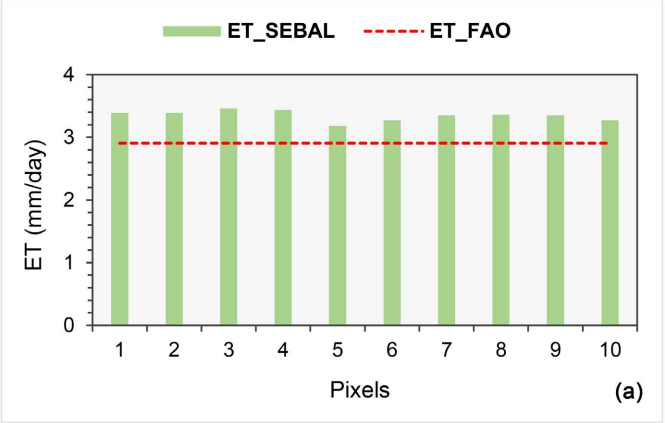

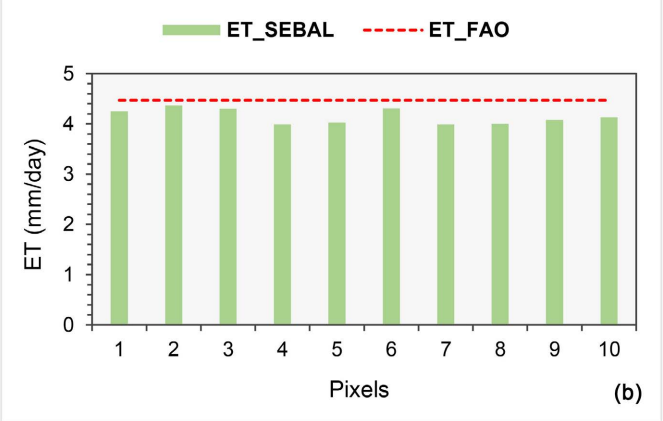

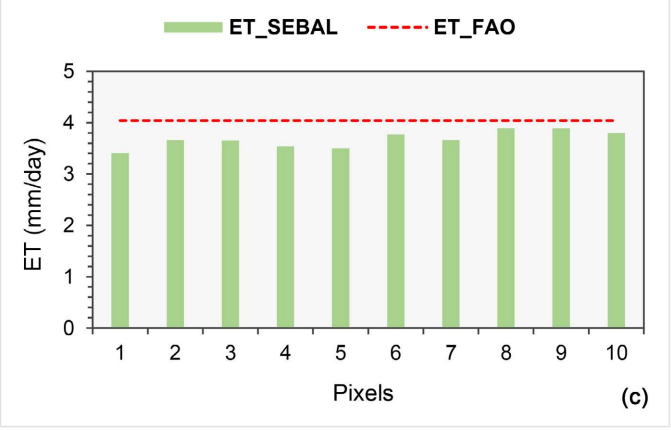

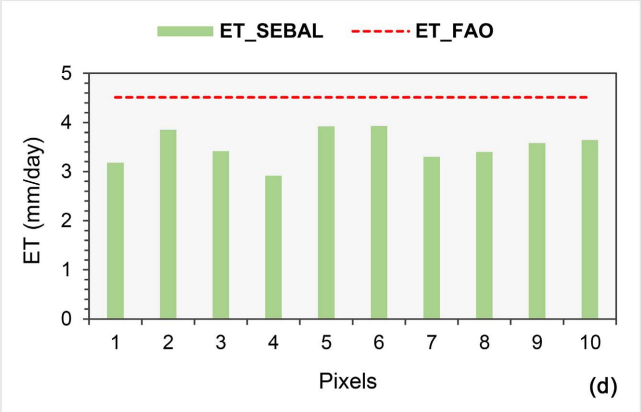

Figure 7. Comparison between the actual SEBAL evapotranspiration obtained for the four satellite images and the rice crop evapotranspiration on the dates of (a) 29 December 2019, (b) 14 January 2020, (c) 30 January 2020 and (d) 15 February 2020.

0.222 mm/day would indicate that the SEBAL model is accurate enough to estimate actual evapotranspiration. [39], reported an RMSE of 1.02 mm/day in estimating ET when results derived from SEBAL were compared to ET values from a water balance model for a sorghum field.

4. Conclusions

In this study, the SEBAL model was used to map the spatial distribution of actual evapotranspiration in the department of Yamoussoukro. A total of four (4) satellite images were used and supported by the FAO method. The spatial variability of evapotranspiration was analyzed while highlighting its sensitivity to the different land cover occupations.

The results indicate that the AET of the area averages 4.92 mm/day, and that at the rice-growing perimeter, the AET ranges from 2.80 to 4.69 mm/day. Also, the analysis of the AET for the different types of land use reveals that water bodies (4.90 mm/day) and flooded vegetation (4.88 mm/day) have the highest values, while the lowest values are observed for bare and built-up soils (2.04 mm/day). Then, it was shown that there was a good agreement between the estimates obtained by SEBAL method and by the FAO-Penman-Monteith method, which makes the algorithm valid. The RMSE between the models were less than or equal to 1.00 mm/day.

This shows the relevance of the application of the remote sensing method in the estimation of evapotranspiration in the study area. Moreover, these results constitute a means of encouraging but also inviting the various actors of the agricultural sector to strengthen their capacities and existing means for a rational use of the available water resources and the use of new agricultural technologies in order to maximize the agricultural yields.

Acknowledgements

This research was funded by the CSRS (Swiss Center for Scientific Research)

through its Strategic Support Program for Scientific Research (PASRES). All the authors would like to thank the Institut National Polytechnique Félix Houphouët-Boigny (INP-HB) of Yamoussoukro in Côte d'Ivoire for its cooperation and support.

Conflicts of Interest

The authors declare no conflicts of interest regarding the publication of this paper.

References

[1] RGPH (2021) Résultats globaux. Institut National de la Satistique (INS), Côte d'Ivoire.

[2] Cordeil, A., Othman, W. and Touré, M. (2009) Evaluation approfondie de la sécurité alimentaire des ménages ruraux en Côte d'Ivoire. Programme alimentaire mondial des Nations Unies, Côte d'Ivoire, Rapport Final.

[3] Macauley, H. and Ramadjita, T. (2015) Les cultures céréalières : Riz, maïs, millet, sorgho et blé. Document de référence, Dakar.

[4] Rahimzadegan, M. and Janani, A. (2019) Estimating Evapotranspiration of Pistachio Crop Based on SEBAL Algorithm Using Landsat 8 Satellite Imagery. *Agricultural Water Management*, **217**, 383-390. https://doi.org/10.1016/j.agwat.2019.03.018

[5] de Lima, C.E.S., de Oliveira Costa, V.S., Galvíncio, J.D., da Silva, R.M. and Santos, C.A.G. (2021) Assessment of Automated Evapotranspiration Estimates Obtained Using the GP-SEBAL Algorithm for Dry Forest Vegetation (Caatinga) and Agricultural Areas in the Brazilian Semiarid Region. *Agricultural Water Management*, **250**, Article ID: 106863. https://doi.org/10.1016/j.agwat.2021.106863

[6] Santos, C.A.G., da Silva, R.M., Silva, A.M. and Brasil Neto, R.M. (2017) Estimation of Evapotranspiration for Different Land Covers in a Brazilian Semi-Arid Region: A Case Study of the Brígida River Basin, Brazil. *Journal of South American Earth Sciences*, **74**, 54-66. https://doi.org/10.1016/j.jsames.2017.01.002

[7] Traore, F. (2007) Méthodes d'estimation de l'évapotranspiration réelle à l'échelle du bassin versant du Kou au Burkina Faso. Ph.D. or Master's Thesis, Université de Liège, Liège.

[8] Pepin, S. and Bourgeois, G. (2012) Outils agrométéorologiques pour la planification de l'irrigation des cultures. https://www.agrireseau.net/grandescultures/documents/Pepin_Bourgeois.pdf

[9] Liou, Y.A. and Kar, S. (2014) Evapotranspiration Estimation with Remote Sensing and Various Surface Energy Balance Algorithms—A Review. *Energies*, 7, 2821-2849. https://doi.org/10.3390/en7052821

[10] Combres, J.C. (1979) Notes sur l'évapotranspiration. *Fruits*, **34**, 359-362.

[11] da Silva, B.B., Mercante, E., Boas, M.A.V., Wrublack, S.C. and Oldoni, L.V. (2018) Satellite-Based ET Estimation Using Landsat 8 Images and SEBAL Model. *RRevista Ciência Agronômica*, **49**, 221-227. https://doi.org/10.5935/1806-6690.20180025

[12] Salifu, T., Agyare, W.A., Kyei-Baffour, N., Mensah, E. and Ofori, E. (2011) Estimating Actual Evapotranspiration Using the SEBAL Model for the Atankwidi and Afram Catchments in Ghana. *International Journal of Applied Agricultural Research*, **6**, 177-193.

[13] Sun, Z.P., *et al.* (2011) Evapotranspiration Estimation Based on the SEBAL Model in

the Nansi Lake Wetland of China. *Mathematical and Computer Modelling*, **54**, 1086-1092. https://doi.org/10.1016/j.mcm.2010.11.039

[14] Nouri, H. (2017) Estimation of Evapotranspiration Based on Surface Energy Balance Algorithm for Land (Sebal) Using Landsat 8 and Modis Images. *Applied Ecology and Environmental Research*, **15**, 1971-1982. https://doi.org/10.15666/aeer/1504_19711982

[15] Ghaderi, A., Dasineh, M., Shokri, M. and Abraham, J. (2020) Estimation of Actual Evapotranspiration Using the Remote Sensing Method and SEBAL Algorithm: A Case Study in Ein Khosh Plain, Iran. *Hydrology*, **7**, Article 36. https://doi.org/10.3390/hydrology7020036

[16] Karra, K., Kontgis, C., Statman-Weil, Z., Mazzariello, J.C., Mathis, M. and Brumby, S.P. (2021) Global Land Use/Land Cover with Sentinel 2 and Deep Learning. 2021 *IEEE International Geoscience and Remote Sensing Symposium IGARSS*, Brussels, 11-16 July 2021, 4704-4707. https://doi.org/10.1109/IGARSS47720.2021.9553499

[17] Allen, R.G., Pereira, L.S., Raes, D. and Smith, M. (1998) Crop Evapotranspiration—Guidelines for Computing Crop Water Requirements—FAO Irrigation and Drainage Paper 56. https://www.researchgate.net/publication/235704197_Crop_evapotranspiration-Guidelines_for_computing_crop_water_requirements-FAO_Irrigation_and_drainage_paper_56

[18] Kergomard, C. (2000) Pratique des corrections atmosphériques en télédétection : Utilisation du logiciel 5S-PC. *Cybergeo*: *European Journal of Geography* http://journals.openedition.org/cybergeo/1679 https://doi.org/10.4000/cybergeo.1679

[19] Staenz, K., Neville, R.A., Clavette, S., Landry, R., White, H.P. and Hitchcock, R. (2002) Retrieval of Surface Reflectance from Hyperion Radiance Data. *IEEE International Geoscience and Remote Sensing Symposium*, Toronto, 24-28 June 2002, 1419-1421. https://doi.org/10.4095/219887

[20] Ghaderi, A., Dasineh, M., Shokri, M. and Abraham, J. (2020) Estimation of Actual Evapotranspiration Using the Remote Sensing Method and SEBAL Algorithm: A Case Study in Ein Khosh Plain, Iran. *Hydrology*, **7**, Article 36. https://doi.org/10.3390/hydrology7020036

[21] Hamimed, A., Abdelkader, K. and Zaagane, M. (2018) Méthodologie d'estimation de l'évapotranspiration et des flux énergétiques de surface à partir des données satellitaires thermiques et des modèles du bilan énergétique. https://www.researchgate.net/publication/328026994

[22] Bastiaanssen, W.G.M., Menenti, M., Feddes, R.A. and Holtslag, A.A.M. (1998) A Remote Sensing Surface Energy Balance Algorithm for Land (SEBAL). 1. Formulation. *Journal of Hydrology*, **212-213**, 198-212. https://doi.org/10.1016/S0022-1694(98)00253-4

[23] Liang, S., *et al.* (2003) Narrowband to Broadband Conversions of Land Surface Albedo: II. Validation. *Remote Sensing of Environment*, **84**, 25-41. https://doi.org/10.1016/S0034-4257(02)00068-8

[24] Rouse, W. and Haas, R.H. (1974) Monitoring Vegetation Systems in the Great Plains with Erts. https://ntrs.nasa.gov/citations/19740022614

[25] Souidi, Z., Hamimed, A., Donze, F., Seddini, A. and Mederbal, K. (2010) Estimation de l'évapotranspiration d'un couvert forestier en Algérie par télédétection. Ph.D. Thesis, Université Montpellier, Montpellier.

[26] Allen, R.G., Tasumi, M. and Trezza, R. (2007) Satellite-Based Energy Balance for Mapping Evapotranspiration with Internalized Calibration (METRIC)—Model. *Journal of Irrigation and Drainage Engineering*, **133**, 380-394. https://doi.org/10.1061/(ASCE)0733-9437(2007)133:4(380)

[27] Allen, R., Tasumi, M., Trezza, R., Bastiaanssen, W. and Waters, R. (2002) Surface Energy Balance Algorithms for Land. Advanced Training and User's Manual-Idaho Implementation.

[28] Hamimed, A. and Khaldi, A. (2000) Utilisation des données satellitaires TM de Landsat pour le suivi de l'état hydrique d'un couvert végétal dans les conditions semi -arides en Algérie. *Teledetection*, **2**, 29-38.

[29] Li, S. and Zhao, W. (2010) Satellite-Based Actual Evapotranspiration Estimation in the Middle Reach of the Heihe River Basin Using the SEBAL Method. *Hydrological Processes*, **24**, 3337-3344. https://doi.org/10.1002/hyp.7748

[30] Kamali, M.I. and Nazari, R. (2018) Determination of Maize Water Requirement Using Remote Sensing Data and SEBAL Algorithm. *Agricultural Water Management*, **209**, 197-205. https://doi.org/10.1016/j.agwat.2018.07.035

[31] Diarra, A. (2017) Suivi de l'évapotranspiration des cultures irriguées du Sud de la Méditerranée par télédétection multi-capteurs et modélisation globale. Master's Thesis, Université Pierre et Marie Curie—Université Cadi Ayyad, Paris.

[32] Bandara, K.M.P.S. (2006) Assessing Irrigation Performance by Using Remote Sensing. Ph.D. Thesis, Wageningen University, Wageningen.

[33] Cai, X.L. and Sharma, B.R. (2010) Integrating Remote Sensing, Census and Weather Data for an Assessment of Rice Yield, Water Consumption and Water Productivity in the Indo-Gangetic River Basin. *Agricultural Water Management*, **97**, 309-316. https://doi.org/10.1016/j.agwat.2009.09.021

[34] Compaore, H. (2023) The Impact of Savannah Vegetation on the Spatial and Temporal Variation of Actual Evapotranspiration in the Volta Basin. https://www.academia.edu/7856159/The_impact_of_savannah_vegetation_on_the_spatial_and_temporal_variation_of_actual_evapotranspiration_in_the_Volta_Basin

[35] Hesadi, H., Behnia, A., AkhoondAli, A.M., Kashefi Pour, S.M., Daneshkar Arasteh, P. and Karimi, A.R. (2022) Estimation of Evapotranspiration of Rangeland Cover Using SEBAL Algorithm in Robat Mahidasht Region Kermanshah Iran. *Journal of Rangeland Science*, **12**, 48-62.

[36] Ochoa-Sánchez, A., Crespo, P., Carrillo-Rojas, G., Sucozhañay, A. and Célleri, R. (2019) Actual Evapotranspiration in the High Andean Grasslands: A Comparison of Measurement and Estimation Methods. *Frontiers in Earth Science*, **7**, Article 433802. https://doi.org/10.3389/feart.2019.00055

[37] Lacharme, M. (2001) Données morphologiques et cycle de la plante. https://www.arid-afrique.org/IMG/pdf/plant%20de%20riz.pdf

[38] de Paiva Lima, E., Sediyama, G.C., Andrade, R.G., Lopes, V.D. and da Silva, B.B. (2014) Evapotranspiração real diária em sub-bacias do Paracatu, utilizando produtos do sensor Modis. *Revista Ceres*, **61**, 17-27. https://doi.org/10.1590/S0034-737X2014000100003

[39] Al Zayed, I.S., Elagib, N.A., Ribbe, L. and Heinrich, J. (2016) Satellite-Based Evapotranspiration over Gezira Irrigation Scheme, Sudan: A Comparative Study. *Agricultural Water Management*, **177**, 66-76. https://doi.org/10.1016/j.agwat.2016.06.027